FRONTIERS OF PHYSICS

RESEARCH ARTICLE
Volume 21 / Issue 4 / 042203 / 2026

Symmetry-guided nonreciprocal transport in non-Hermitian scattering systems: Parity–flux reversal effects

Xi Zhang, TianMeng Sun-Huo, XiZheng Zhang†

College of Physics and Materials Science, Tianjin Normal University, Tianiin 300387, China
Corresponding author. E-mail: †zhangxz@tjnu.edu.cn
Received July 15, 2025; accepted September 10, 2025

ABSTRACT

Nonreciprocity plays a pivotal role in the design of optical and quantum devices. A key mechanism for achieving it lies in the breaking of Lorentz reciprocity. In this paper, we systematically investigate the scattering properties of a non-Hermitian system composed of an arbitrary-dimensional scattering center coupled to two semi-infinite leads. We first propose a general theorem that elucidates how symmetry constrains the transmission and reflection amplitudes. We show that parity–time ($\mathcal{PT}$) symmetric systems can still exhibit reciprocal transmission despite the presence of non-Hermitian terms. The introduction of a magnetic flux that preserves parity symmetry and flux inversion symmetry can break Lorentz reciprocity and thus enable nonreciprocal transport. Based on detailed symmetry analysis, we construct a series of minimal models that demonstrate unidirectional transmission. Our results provide new insights into the mechanisms of nonreciprocal scattering and offer a theoretical foundation for the development of optical diodes and quantum isolators in non-Hermitian systems.

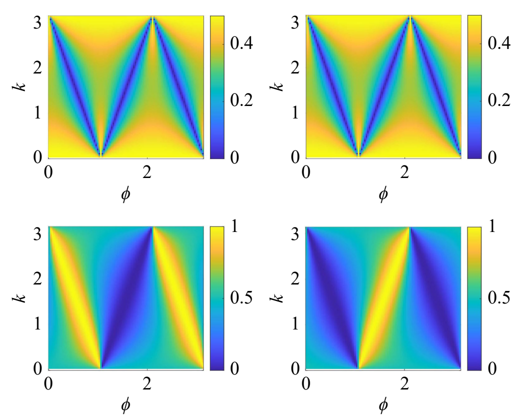

Keywords non-Hermitian systems, nonreciprocal transmission

1 Introduction

Nonreciprocal transport, where a system exhibits asymmetric transmission properties for waves incident from opposite directions, has garnered growing attention in recent years due to its fundamental significance and broad technological applications [1–8]. In contrast to reciprocal systems, where the transmission properties are symmetric with respect to the direction of incidence, nonreciprocal systems allow for the selective control of wave propagation. This property is pivotal for the development of next-generation photonic and quantum devices, including isolators, circulators, unidirectional amplifiers, and topological lasers [9–14]. Achieving robust nonreciprocity is thus crucial for realizing advanced information processing, protected signal routing, and enhanced device functionality in both classical and quantum domains.

Recent experimental progress has brought nonreciprocal physics to the forefront of photonics and quantum technology [15–20]. In photonic systems, synthetic magnetic fields and temporal modulation have been used to break Lorentz reciprocity, enabling unidirectional wave propagation in optical resonators, photonic lattices, and metamaterials [21–27]. Similarly, in quantum platforms such as superconducting circuits and ultracold atoms, engineered dissipation and non-Hermitian Hamiltonians have been employed to realize controllable gain and loss, leading to nonreciprocal transport at the quantum level [28–33]. These advancements not only expand the scope of

*Special Topic: Non-Hermitian Physics (Eds.: Peng Xue, Lan Yang & Wu-Ming Liu).

Higher Education Press

https://doi.org/10.15302/frontphys.2026.042203

controllable transport phenomena but also open new avenues for the realization of symmetry-protected non-Hermitian dynamics.

In this work, we systematically investigate the scattering behavior of a class of non-Hermitian systems composed of a finite scattering center and two semi-infinite tight-binding leads. By introducing complex on-site potentials and a tunable magnetic flux into the scattering center, we explore how various symmetry constraints, particularly parity–time ($\mathcal{PT}$) and parity-magnetic-flux reversal ($\mathcal{PM_F}$) symmetries, govern the reciprocity of transmission and reflection. Here, we define the parity–flux-reversal ($\mathcal{PM_F}$) symmetry as the invariance of the system under the combined operation of spatial inversion ($\mathcal{P}$) and magnetic flux reversal ($\mathcal{M_F}$). Our analysis leads to several key findings. We rigorously prove a general relation between the symmetry of the system and the reciprocity of scattering amplitudes. Importantly, we demonstrate that the presence of $\mathcal{PM_F}$ symmetry does not necessarily guarantee nonreciprocal transport, highlighting the need for symmetry breaking beyond traditional $\mathcal{PT}$ paradigms. Furthermore, we identify a series of microscopic configurations that allow for perfect unidirectional transmission and amplification under specific parameter conditions.

Unlike previous studies that focused primarily on $\mathcal{PT}$-symmetric non-Hermitian systems, our results highlight that even systems with the combined parity–flux-reversal ($\mathcal{PM_F}$) symmetry can display nonreciprocal transport. This demonstrates that $\mathcal{PM_F}$ symmetry provides a new route beyond $\mathcal{PT}$ constraints,enriching the overall understanding of directional scattering.

The paper is organized as follows. In Section 2, we present a general theoretical framework for symmetry analysis in non-Hermitian scattering systems and derive constraints on the scattering amplitudes. In Section 3, we construct a minimal tight-binding model with tunable complex potentials and magnetic flux, and analyze its scattering properties under various symmetry classes. Section 4 explores multiple representative configurations where nonreciprocity emerges, supported by both analytical expressions and numerical simulations. Finally, Section 5 summarizes the main results and discusses their implications for designing nonreciprocal quantum and photonic devices.

2 Scattering states and symmetry constraints

We consider a one-dimensional scattering system with only two channels, corresponding to left and right incidence. The scattering center may have arbitrary spatial dimension, but only one-dimensional asymptotic channels are assumed as sketched in Fig. 1. The two linearly independent scattering eigenstates are given by

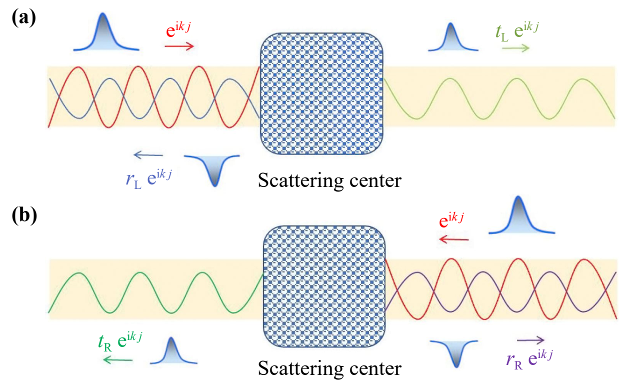

Fig. 1 Schematic illustration of the scattering system. It consists of two one-dimensional scattering channels (yellow shaded regions) and a central scattering region (blue grid area), which can have arbitrary geometry or dimensionality. Panels **(a)** and **(b)** correspond to right- and left-incident plane waves, respectively. The analysis focuses on the role of symmetry in determining the transmission properties, with particular attention to unidirectional transport, which forms the basis for optical and quantum information networks.

$$f_{\mathrm{L}}^{k}(j)=\begin{cases}\mathrm{e}^{\mathrm{i}kj}+r_{\mathrm{L}}^{k}\mathrm{e}^{-\mathrm{i}kj}, & j\ll 0,\\ t_{\mathrm{L}}^{k}\mathrm{e}^{\mathrm{i}kj}, & j\gg 0,\end{cases}\tag{1}$$

$$f_{\mathrm{R}}^{k}(j)=\begin{cases}t_{\mathrm{R}}^{k}\mathrm{e}^{-\mathrm{i}kj}, & j\ll 0,\\ \mathrm{e}^{-\mathrm{i}kj}+r_{\mathrm{R}}^{k}\mathrm{e}^{\mathrm{i}kj}, & j\gg 0.\end{cases}\tag{2}$$

By taking linear combinations of degenerate states [6], we derive the relations

$$t_{\mathrm{L}}^{-k}t_{\mathrm{R}}^{k}+r_{\mathrm{L}}^{-k}r_{\mathrm{L}}^{k}=1,\tag{3}$$

$$t_{\mathrm{L}}^{-k}r_{\mathrm{R}}^{k}+r_{\mathrm{L}}^{-k}t_{\mathrm{L}}^{k}=0.\tag{4}$$

2.1 Parity symmetry

Under the action of the parity operator $\mathcal{P}$

$$\mathcal{P}:j\rightarrow -j,\tag{5}$$

applying $\mathcal{P}$ to $f_{\mathrm{L}}^{k}(j)$ and comparing with $f_{\mathrm{R}}^{k}(j)$ gives:

$$r_{\mathrm{R}}^{k}=r_{\mathrm{L}}^{k},\quad t_{\mathrm{R}}^{k}=t_{\mathrm{L}}^{k}.\tag{6}$$

These relations reflect the intrinsic symmetry of space and hold irrespective of probability conservation.

2.2 Time-reversal symmetry

For a system with time-reversal symmetry, the operator satisfies $\mathcal{T}\mathrm{i}\mathcal{T}^{-1}=-\mathrm{i}$. Comparing $f_{\mathrm{L,R}}^{-k}(j)$ with $(f_{\mathrm{L,R}}^{k}(j))^{*}$ leads to

$$r_{\mathrm{L,R}}^{-k}=(r_{\mathrm{L,R}}^{k})^{*},\quad t_{\mathrm{L,R}}^{-k}=(t_{\mathrm{L,R}}^{k})^{*}.\tag{7}$$

Together with probability conservation,

$$|r^k_{\mathrm{L,R}}|^2 + |t^k_{\mathrm{L,R}}|^2 = 1, \tag{8}$$

this yields

$$t^k_{\mathrm{R}} = t^k_{\mathrm{L}}, \quad |r^k_{\mathrm{R}}| = |r^k_{\mathrm{L}}|, \tag{9}$$

implying reciprocal transport in any time-reversal symmetric Hermitian system.

2.3 $\mathcal{PT}$ symmetry

For a $\mathcal{PT}$-symmetric scatterer, acting $\mathcal{PT}$ on $f^k_{\mathrm{R}}(j)$ and comparing with $f^k_{\mathrm{L}}(j)$ yields

$$(r^k_{\mathrm{R}})^* = r^{-k}_{\mathrm{L}}, \quad (t^k_{\mathrm{R}})^* = t^{-k}_{\mathrm{L}}. \tag{10}$$

Combining with Eq. (3), we find

$$|t^k_{\mathrm{L}}| = |t^k_{\mathrm{R}}|, \tag{11}$$

indicating that transmission remains reciprocal even when probability is not conserved, as in non-Hermitian systems.

2.4 Breaking reciprocity via magnetic flux

To break reciprocity, we introduce a Hermitian magnetic flux ϕ that breaks time-reversal symmetry. We define the magnetic-flux-reversal operator $\mathcal{M}_{\mathcal{F}}$ such that

$$\mathcal{M}_{\mathcal{F}} : \phi \to -\phi. \tag{12}$$

The operator $\mathcal{M}_{\mathcal{F}}$ acts only on the magnetic flux, while leaving the time coordinate unchanged. When combined with parity $\mathcal{P}$, the joint $\mathcal{PM}_{\mathcal{F}}$ symmetry imposes nontrivial constraints on scattering amplitudes. The Hamiltonian then transforms as

$$\mathcal{M}_{\mathcal{F}} H(\phi) \mathcal{M}_{\mathcal{F}}{}^{-1} = H(-\phi), \tag{13}$$

$$\mathcal{PM}_{\mathcal{F}} H(\phi) (\mathcal{PM}_{\mathcal{F}})^{-1} = H(\phi). \tag{14}$$

The invariance under $\mathcal{PM}_{\mathcal{F}}$ implies that the transformed wavefunctions must also be physical solutions of $H(\phi)$. Applying $\mathcal{PM}_{\mathcal{F}}$ to the left-incident wave $f^k_{\mathrm{L}}(j,\phi)$

$$\mathcal{PM}_{\mathcal{F}} f^k_{\mathrm{L}}(j) = \begin{cases} \mathrm{e}^{-\mathrm{i}kj} + r^k_{\mathrm{L}}(-\phi)\mathrm{e}^{\mathrm{i}kj}, & j \gg 0, \\ t^k_{\mathrm{L}}(-\phi)\mathrm{e}^{-\mathrm{i}kj}, & j \ll 0, \end{cases} \tag{15}$$

and comparing with $f^k_{\mathrm{R}}(j,\phi)$, we find

$$t^k_{\mathrm{L}}(-\phi) = t^k_{\mathrm{R}}(\phi), \quad r^k_{\mathrm{L}}(-\phi) = r^k_{\mathrm{R}}(\phi). \tag{16}$$

When $\phi \rightleftarrows -\phi$, Eq. (16) still holds.

Eq. (16) shows that the transmission and reflection amplitudes at flux $-\phi$ are related to those at flux ϕ by parity exchange, independent of time-reversal invariance. We define systems satisfying Eq. (16) as possessing $\mathcal{PM}_{\mathcal{F}}$ symmetry.

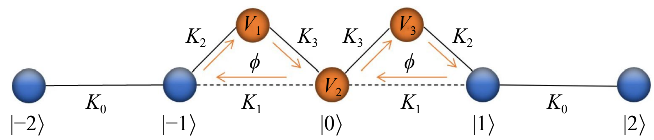

Fig. 2 A scattering center governed jointly by magnetic flux (ϕ) and complex potential (V).

In the next section, we explore the impact of introducing flux into a non-Hermitian scattering center and demonstrate how varying the position and magnitude of the complex potential enables controllable nonreciprocal transport, including perfect unidirectional reflectionless transmission at specific flux values.

3 Model hamiltonian and scattering solutions

We now consider a tight-binding model consisting of a one-dimensional chain with nearest-neighbor hopping. The full Hamiltonian is given by

$$H = H_{\mathrm{L}} + H_{\mathrm{C}} + H_{\mathrm{R}}, \tag{17}$$

where H_{L} and H_{R} describe the semi-infinite leads (scattering channels) on the left and right of the scattering center, respectively, while H_{C} captures the scattering center with possibly non-Hermitian on-site potentials and synthetic magnetic flux ϕ. The lead Hamiltonians take the standard form:

$$H_{\mathrm{L}} = -\kappa_0 \sum_j \left(a^\dagger_j a_{j+1} + \mathrm{H.c.} \right), \tag{18}$$

$$H_{\mathrm{R}} = -\kappa_0 \sum_j \left(a^\dagger_j a_{j+1} + \mathrm{H.c.} \right). \tag{19}$$

The scattering center is modeled by

$$\begin{aligned} H_{\mathrm{C}} = & -\mathrm{e}^{-\mathrm{i}\phi}(\kappa_2 b^\dagger_1 a_{-1} + \kappa_3 b^\dagger_2 b_1 + \kappa_1 a^\dagger_{-1} b_2 \\ & + \kappa_3 b^\dagger_3 b_2 + \kappa_2 a^\dagger_1 b_3 + \kappa_1 b^\dagger_2 a_1) + \mathrm{H.c.} \\ & + V_1 b^\dagger_1 b_1 + V_2 b^\dagger_2 b_2 + V_3 b^\dagger_3 b_3, \end{aligned} \tag{20}$$

where the on-site potentials V_m $(m = 1,2,3)$ can be complex-valued, introducing non-Hermiticity into the system. The operators $a^\dagger_j$ (a_j) and $b^\dagger_j$ (b_j) create (annihilate) bosons or fermions on the leads and center sites, respectively. The notation H.c. denotes Hermitian conjugates of the hopping terms, and κ_ℓ $(\ell = 0,1,2,3)$ are real hopping amplitudes. The magnetic flux ϕ is embedded into the hopping terms via the phase factor $\mathrm{e}^{-\mathrm{i}\phi}$. In particular, notice that the parameter ϕ represents an effective magnetic flux that can be physically realized in different platforms. For instance, in photonic lattices ϕ

can be engineered by introducing phase delays in ring resonator arrays [34], in ultracold atom systems it can be simulated through laser-assisted tunneling that induces synthetic gauge fields [35], and in superconducting circuits it naturally arises from externally applied magnetic fluxes [36, 37]. These examples illustrate that the flux parameter in our model is not merely a mathematical abstraction, but has concrete realizations in a variety of experimental settings.

We solve this system using the Bethe Ansatz method. The single-particle eigenstate satisfies

$$H|k\rangle = E|k\rangle, \tag{21}$$

with plane-wave dispersion $E=-2\kappa_0\cos k$ in the leads. The general form of the wavefunction reads

$$|k\rangle = \sum_j f_j|j\rangle + \sum_l g_l|l\rangle, \tag{22}$$

where f_j and g_l denote amplitudes on the scattering channels and scattering center, respectively. The asymptotic form of f_j follows Eqs. (1) and (2). Substituting the ansatz into Eq. (21), we obtain the following coupled equations:

$$\begin{aligned}
Ef_{-1} &= -\kappa_0 f_{-2} - e^{i\phi}\kappa_2 g_1 - e^{-i\phi}\kappa_1 g_2,\\
Ef_1 &= -\kappa_0 f_2 - e^{-i\phi}\kappa_2 g_3 - e^{i\phi}\kappa_1 g_2,\\
(E-V_1)g_1 &= -e^{i\phi}\kappa_3 g_2 - e^{-i\phi}\kappa_2 f_{-1},\\
(E-V_3)g_3 &= -e^{i\phi}\kappa_2 f_1 - e^{-i\phi}\kappa_3 g_2,\\
(E-V_2)g_2 &= -e^{-i\phi}\kappa_3 g_1 - e^{i\phi}\kappa_3 g_3\\
&\quad - e^{i\phi}\kappa_1 f_{-1} - e^{-i\phi}\kappa_1 f_1.
\end{aligned} \tag{23}$$

By solving the coupled equations Eq. (23) to eliminate the central state amplitudes g_l, equations for f_j are obtained, from which the analytical expressions for the reflection and transmission amplitudes can be derived.

$$r_{\mathrm{L}} = \frac{\lambda[\mu'\varsigma - \beta\beta'(E-V_1)] - \alpha\alpha'\mu'(E-V_3)}{e^{2ik}[\alpha\alpha'\mu'(E-V_3) - \lambda'\mu'\varsigma + \beta\beta'\lambda'(E-V_1)]}, \tag{24}$$

$$r_{\mathrm{R}} = \frac{\lambda'[\mu\varsigma - \beta\beta'(E-V_1)] - \alpha\alpha'\mu(E-V_3)}{e^{2ik}[\alpha\alpha'\mu'(E-V_3) - \lambda'\mu'\varsigma + \beta\beta'\lambda'(E-V_1)]}, \tag{25}$$

$$t_{\mathrm{L}} = \frac{-2i\kappa_0\alpha'\beta\sin k(E-V_1)(E-V_3)}{e^{2ik}[\alpha\alpha'\mu'(E-V_3) - \lambda'\mu'\varsigma + \beta\beta'\lambda'(E-V_1)]}, \tag{26}$$

$$t_{\mathrm{R}} = \frac{-2i\kappa_0\alpha\beta'\sin k(E-V_1)(E-V_3)}{e^{2ik}[\alpha\alpha'\mu'(E-V_3) - \lambda'\mu'\varsigma + \beta\beta'\lambda'(E-V_1)]}. \tag{27}$$

Here we define:

$$\begin{aligned}
\alpha &= e^{2i\phi}\kappa_2\kappa_3 - e^{-i\phi}\kappa_1(E-V_1),\\
\beta &= e^{-2i\phi}\kappa_2\kappa_3 - e^{i\phi}\kappa_1(E-V_3),\\
\lambda &= -\kappa_0(E-V_1)e^{ik} - \kappa_2^2,\\
\mu &= -\kappa_0(E-V_3)e^{ik} - \kappa_2^2,\\
\varsigma &= (E-V_1)(E-V_2)(E-V_3) - \kappa_3^2(2E-V_1-V_3).
\end{aligned} \tag{28}$$

Under flux reversal $\phi\to-\phi$:

$$\alpha\to\alpha', \beta\to\beta', \tag{29}$$

wavevector inversion $k\to-k$:

$$\lambda\to\lambda', \mu\to\mu'. \tag{30}$$

4 Transmission under different on-site potential configurations

Building on the above symmetry analysis, we now investigate how different choices of the complex onsite potentials V_m affect the transmission coefficients. In particular, we propose schemes for achieving nonreciprocal transport by appropriately engineering the scattering center. Unless otherwise stated, we set all hopping amplitudes to unity: $\kappa_1=\kappa_2=\kappa_3=\kappa_0=1$.

4.1 Reciprocity and symmetry breaking

First, we assume that all potentials V_m are real-valued (denoted V_r), the system is Hermitian. The Hamiltonian simplifies to

$$\begin{aligned}
H_{\mathrm{C}}^{(\mathrm{Herm})} = &-e^{-i\phi}(b_1^\dagger a_{-1} + b_2^\dagger b_1 + a_{-1}^\dagger b_2\\
&+ b_3^\dagger b_2 + a_1^\dagger b_3 + b_2^\dagger a_1) + \mathrm{H.c.}\\
&+ V_r(b_1^\dagger b_1 + b_2^\dagger b_2 + b_3^\dagger b_3).
\end{aligned} \tag{31}$$

In this case, the system exhibits reciprocal transport, i.e., $|t_{\mathrm{L}}^k| = |t_{\mathrm{R}}^k|$, regardless of the value of ϕ, due to the underlying $\mathcal{PT}$ symmetry.

Next, consider a non-Hermitian case with $\phi=0$ and complex symmetric potentials $V_1=V_3=-e^{i\gamma}$, $V_2=0$, leading to

$$\begin{aligned}
H_{--} = &-(b_1^\dagger a_{-1} + b_2^\dagger b_1 + a_{-1}^\dagger b_2\\
&+ b_3^\dagger b_2 + a_1^\dagger b_3 + b_2^\dagger a_1) + \mathrm{H.c.}\\
&- e^{i\gamma}(b_1^\dagger b_1 + b_3^\dagger b_3).
\end{aligned} \tag{32}$$

This system satisfies $\mathcal{P}H_{--}\mathcal{P}^{-1} = H_{--}$, and hence also exhibits reciprocal transmission.

For the final model, we consider a configuration with onsite potentials $V_1=V_3=0$ and $V_2=-e^{i\gamma}$. The corresponding Hamiltonian of the scattering center is given by

$$\begin{aligned}H_{\mathrm{C}}^{(\mathcal{PM}_{\mathcal{F}})} =& -\mathrm{e}^{-\mathrm{i}\phi}(b_1^\dagger a_{-1} + b_2^\dagger b_1 + a_{-1}^\dagger b_2 \\ &+ b_3^\dagger b_2 + a_1^\dagger b_3 + b_2^\dagger a_1) + \mathrm{H.c.} \\ &- \mathrm{e}^{\mathrm{i}\gamma} b_2^\dagger b_2. \end{aligned} \tag{33}$$

This Hamiltonian is invariant under the combined $\mathcal{PM}_{\mathcal{F}}$ transformation, i.e., $\mathcal{PM}_{\mathcal{F}} H_{\mathrm{C}}^{(\mathcal{PM}_{\mathcal{F}})} (\mathcal{PM}_{\mathcal{F}})^{-1} = H_{\mathrm{C}}^{(\mathcal{PM}_{\mathcal{F}})}$, which guarantees the relation $t_{\mathrm{L}}(-\phi) = t_{\mathrm{R}}(\phi)$, as dictated by the symmetry constraint Eq. (16). To illustrate this point, we evaluate the scattering amplitudes analytically at the specific wavevector $k=\gamma$. The resulting reflection and transmission coefficients are

$$r_{\mathrm{L}}^{\mathcal{PM}_{\mathcal{F}}} = r_{\mathrm{R}}^{\mathcal{PM}_{\mathcal{F}}} = \frac{\cos 2k(\mathrm{e}^{-\mathrm{i}k} - 2\delta E\cos k)}{\delta E - \mathrm{e}^{-3\mathrm{i}k}\cos 2k}, \tag{34}$$

$$t_{\mathrm{L}}^{\mathcal{PM}_{\mathcal{F}}} = \frac{\mathrm{i}E\sin 2k(\mathrm{e}^{-2\mathrm{i}\phi} - \mathrm{e}^{\mathrm{i}\phi}E)^2}{\delta E - \mathrm{e}^{-3\mathrm{i}k}\cos 2k}, \tag{35}$$

$$t_{\mathrm{R}}^{\mathcal{PM}_{\mathcal{F}}} = \frac{\mathrm{i}E\sin 2k(\mathrm{e}^{2\mathrm{i}\phi} - \mathrm{e}^{-\mathrm{i}\phi}E)^2}{\delta E - \mathrm{e}^{-3\mathrm{i}k}\cos 2k}. \tag{36}$$

Here we define:

$$\delta = 1 - 2E\cos 3\phi + E^2. \tag{37}$$

It is evident that under $\phi \to -\phi$, the relation $t_{\mathrm{L}}^{\mathcal{PM}_{\mathcal{F}}}(\phi) = t_{\mathrm{R}}^{\mathcal{PM}_{\mathcal{F}}}(-\phi)$ holds, confirming the symmetry constraint. Nevertheless, we also find that

$$|t_{\mathrm{L}}^{\mathcal{PM}_{\mathcal{F}}}(\phi)| = |t_{\mathrm{R}}^{\mathcal{PM}_{\mathcal{F}}}(\phi)|, \tag{38}$$

which indicates that the system may still exhibit symmetric transmission even when constrained by $\mathcal{PM}_{\mathcal{F}}$ symmetry. This is because Eq. (16) only imposes that the transmission amplitudes are equivalent under magnetic flux sign reversal, rather than strictly requiring $|t_{\mathrm{L}}(\phi)| = |t_{\mathrm{R}}(\phi)|$. Therefore, $\mathcal{PM}_{\mathcal{F}}$ symmetry serves as a permissive condition rather than a determinative one for achieving nonreciprocal transport: it enables the possibility of directionality but cannot guarantee its occurrence. In Fig. 3, we demonstrate this point by comparing $t_{\mathrm{L}}^{\mathcal{PM}_{\mathcal{F}}}$ and $t_{\mathrm{R}}^{\mathcal{PM}_{\mathcal{F}}}$ for the same magnetic flux.

While $\mathcal{PM}_{\mathcal{F}}$ symmetry by itself does not guarantee non-reciprocal transmission, it can accommodate reciprocity breaking under specific conditions. In particular, reciprocity breaking emerges when the microscopic implementation of $\mathcal{PM}_{\mathcal{F}}$ symmetry is combined with mechanisms that inherently distinguish forward and backward propagation. Two such mechanisms are:

i) Magnetic flux

A nonzero Peierls phase (magnetic flux) modifies the complex hopping amplitudes in a $\mathcal{PM}_{\mathcal{F}}$-symmetric system without violating the combined parity–charge-conjugation constraint. This flux breaks time-reversal symmetry, which is a sufficient condition for the scattering matrix to become non-reciprocal in general.

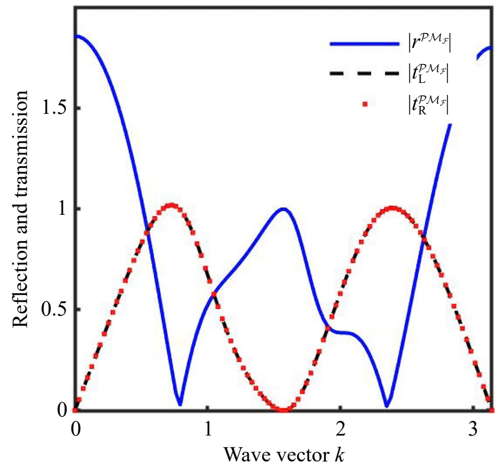

Fig. 3 Scattering probabilities as functions of the wavevector k under the parameter setting $V_1 = V_3 = 0$, $V_2 = -\mathrm{e}^{\mathrm{i}\gamma}$, $k = \gamma \in (0, \pi)$, and magnetic flux $\phi_{\mathrm{c}} = 4\pi/9$. The reflection probability $|r^{\mathcal{PM}_{\mathcal{F}}}|$ and the transmission probabilities $|t_{\mathrm{L}}^{\mathcal{PM}_{\mathcal{F}}}|$ and $|t_{\mathrm{R}}^{\mathcal{PM}_{\mathcal{F}}}|$ are plotted. Although the system preserves the $\mathcal{PM}_{\mathcal{F}}$ symmetry, the transport remains reciprocal in this regime, as evidenced by the equality $|t_{\mathrm{L}}^{\mathcal{PM}_{\mathcal{F}}}| = |t_{\mathrm{R}}^{\mathcal{PM}_{\mathcal{F}}}|$ across the entire range of k.

ii) Spatial distribution of gain/loss

In non-Hermitian systems, balanced gain and loss can be arranged in a manner that preserves $\mathcal{PM}_{\mathcal{F}}$ symmetry but changes the relative amplification/attenuation experienced by waves traveling in opposite directions. The effect is especially pronounced when the gain/loss profile is asymmetric with respect to the system's scattering center, even though the $\mathcal{PM}_{\mathcal{F}}$ transformation maps the Hamiltonian to its negative complex conjugate.

The interplay of these two ingredients — magnetic flux and asymmetric gain/loss — allows $\mathcal{PM}_{\mathcal{F}}$-symmetric systems to support non-reciprocal and even amplified transport. Importantly, $\mathcal{PM}_{\mathcal{F}}$ symmetry constrains the structure of the scattering matrix but does not enforce its reciprocity.

To realize the non-reciprocal transmission, we will consider five representative configurations of the scattering center to illustrate how synthetic magnetic flux ϕ and complex potentials V_j cooperatively influence reciprocity.

4.2 Nonreciprocal transport under symmetry and complex potentials

4.2.1 Symmetric complex potentials with nonzero flux

i) Model with uniform loss: $V_1 = V_3 = -\mathrm{e}^{\mathrm{i}\gamma}$, $V_2 = 0$

The scattering center Hamiltonian takes the form

$$H_{\mathrm{C}_1} = -\mathrm{e}^{-\mathrm{i}\phi}(b_1^\dagger a_{-1} + b_2^\dagger b_1 + a_{-1}^\dagger b_2 + b_3^\dagger b_2 + a_1^\dagger b_3 + b_2^\dagger a_1) + \mathrm{H.c.} - \mathrm{e}^{\mathrm{i}\gamma}(b_1^\dagger b_1 + b_3^\dagger b_3), \tag{39}$$

where the complex potentials are symmetrically distributed about the central site. For the specific case $\gamma = k$, the analytical expressions for the scattering amplitudes are obtained as

$$r_{\mathrm{L}_1,\mathrm{R}_1} = \frac{\mathrm{e}^{-2\mathrm{i}k}(\cos k + \cos 3\phi)}{(\cos 2k - 1)\mathrm{e}^{-\mathrm{i}k} - 2(\cos k + \cos 3\phi)}, \tag{40}$$

$$t_{\mathrm{L}_1}(\phi) = t_{\mathrm{R}_1}(-\phi) = \frac{\mathrm{e}^{-\mathrm{i}k}(\mathrm{e}^{-2\mathrm{i}\phi} + \mathrm{e}^{\mathrm{i}\phi}\mathrm{e}^{-\mathrm{i}k})^2}{2(\cos 2k - 1)\mathrm{e}^{-\mathrm{i}k} - 4(\cos k + \cos 3\phi)}. \tag{41}$$

These results satisfy the symmetry relation in Eq. (16), and confirm that the reflection probabilities for left and right incidence are always identical. Figures 4(a) and (b) show the reflection probabilities for left and right incident wave packets, respectively, while Figs. 4(c) and (d) display the corresponding transmission probabilities.

Although the non-Hermiticity is $\mathcal{P}$-symmetric, the presence of magnetic flux ϕ breaks Lorentz reciprocity, resulting in direction-dependent transport. Notably, along the blue curve in Fig. 4(a), both reflection amplitudes vanish, $r_{\mathrm{L}_1} = r_{\mathrm{R}_1} = 0$. At these parameter values, one can always identify situations in the transmission plots where one transmission probability is unity while the other is zero. For instance, for $\phi \in [0, \frac{\pi}{3}] \cup [\frac{2\pi}{3}, \pi]$, and $|r_{\mathrm{L}_1}| = |r_{\mathrm{R}_1}| = 0$, we find $|t_{\mathrm{L}_1}| = 1$, and $|t_{\mathrm{R}_1}| = 0$ indicating perfect transmission from the left and complete suppression from the right. Conversely, for $\phi \in (\frac{\pi}{3}, \frac{2\pi}{3})$ with vanishing reflection, we observe $|t_{\mathrm{L}_1}| = 0$, and $|t_{\mathrm{R}_1}| = 1$. We refer to this phenomenon as unidirectional reflectionless transport, where the wave is fully transmitted from one side while being completely blocked from the other. Such behavior provides a mechanism for robust direction-selective control of wave propagation. We further verify this feature numerically for various wavevectors $k = \frac{\pi}{2}, \frac{\pi}{3}, \frac{\pi}{4}, \frac{\pi}{5}, \frac{\pi}{6}$, and $|r_{\mathrm{L}_1,\mathrm{R}_1}| = 0$. As shown in Fig. 5, the scattering amplitudes clearly display the effect of non-Hermitian potentials. In the Hermitian limit, the system conserves energy for all values of ϕ, satisfying $|r|^2 + |t|^2 = 1$. In the non-Hermitian regime, however, complex potentials generally induce partial absorption or amplification, so that $|r|^2 + |t|^2 \neq 1$ for generic ϕ. Remarkably, there exist discrete parameter points (e.g., $r = 0, t = 1$), where the effective absorption vanishes. Each of these points corresponds to a configuration in which transmission is completely suppressed from one side while perfect transmission occurs from the other. In such cases, the system satisfies probability conservation.

ii) Model with uniform loss: $V_1 = V_2 = V_3 = -\mathrm{e}^{\mathrm{i}\gamma}$

The Hamiltonian of the scattering center is given as

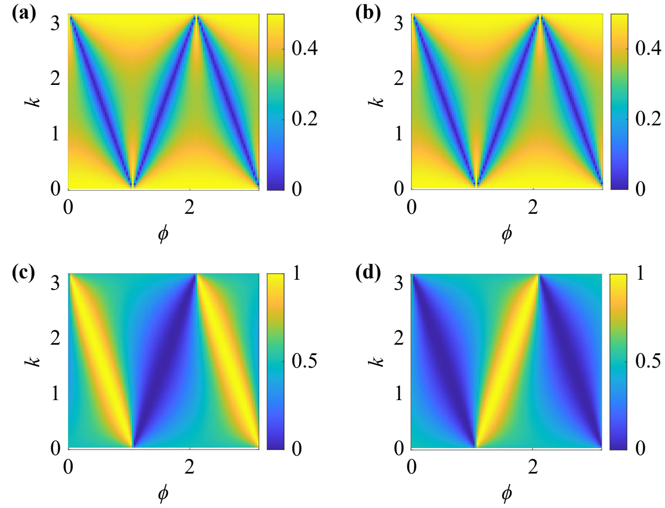

Fig. 4 Scattering probability distributions for the asymmetric scattering model under the parameter conditions $V_1 = V_3 = -\mathrm{e}^{\mathrm{i}\gamma}$, $V_2 = 0$, $k = \gamma \in (0, \pi)$, and $\phi \in (0, \pi)$. **(a)** Left reflection probability $|r_{\mathrm{L}_1}|$; **(b)** right reflection probability $|r_{\mathrm{R}_1}|$; **(c)** left transmission probability $|t_{\mathrm{L}_1}|$; **(d)** right transmission probability $|t_{\mathrm{R}_1}|$. The blue dip regions in panels (a) and (b) ($|r_{\mathrm{L}_1/\mathrm{R}_1}| = 0$) mark the zero-reflection conditions, while the yellow highlighted regions in panels (c) and (d) ($|t_{\mathrm{L}_1/\mathrm{R}_1}| = 1$) indicate ideal full-transmission states. When the parameters lie along the blue contour lines in (a) or (b), the system exhibits perfect unidirectional transmission in which one side supports unit transmission while the opposite side is completely suppressed. The direction of this nonreciprocal transport can be dynamically controlled by tuning the magnetic flux ϕ.

$$H_{\mathrm{C}_2} = H_{\mathrm{C}_1} - \mathrm{e}^{\mathrm{i}\gamma} b_2^\dagger b_2. \tag{42}$$

Obviously, it respects the combined $\mathcal{PM}_{\mathcal{F}}$ symmetry. For $\gamma = k$, the corresponding scattering amplitudes are obtained as

$$r_{\mathrm{L}_2} = r_{\mathrm{R}_2} = -\frac{\cos k + \cos 3\phi}{\mathrm{i}\sin k + 2\mathrm{e}^{\mathrm{i}k} + 2\mathrm{e}^{2\mathrm{i}k}\cos 3\phi}, \tag{43}$$

$$t_{\mathrm{L}_2}(\phi) = t_{\mathrm{R}_2}(-\phi) = -\frac{(\mathrm{e}^{-2\mathrm{i}\phi} + \mathrm{e}^{\mathrm{i}\phi}\mathrm{e}^{-\mathrm{i}k})^2}{2\mathrm{i}\mathrm{e}^{-\mathrm{i}k}\sin k + 4 + 4\mathrm{e}^{\mathrm{i}k}\cos 3\phi}. \tag{44}$$

These expressions satisfy the $\mathcal{PM}_{\mathcal{F}}$-symmetric relation of Eq. (16). Numerical simulations of the scattering behavior are shown in Fig. 6. As in the previous model, a unidirectional reflectionless phenomenon is again observed along the blue contour in Fig. 7, where $|r_{\mathrm{L}_2}| = |r_{\mathrm{R}_2}| = 0$. However, in contrast to Model 1, here the transmission is imperfect even when reflection vanishes. Specifically, at points along the zero-reflection contour, one transmission amplitude is zero while the other is less than unity, i.e., $|t_{\mathrm{L}_2}| < 1$ and $|t_{\mathrm{R}_2}| = 0$ (or vice versa). This indicates that part of the incident

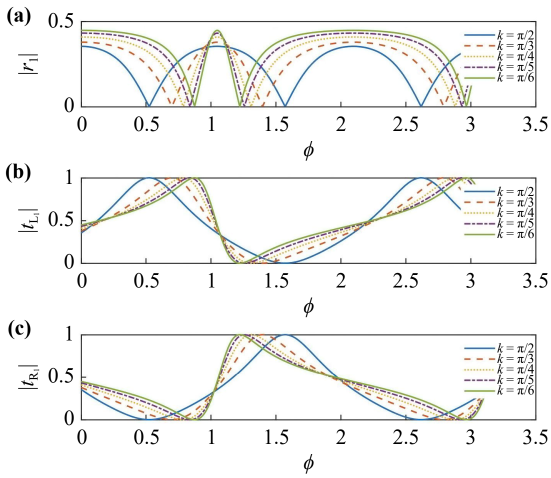

Fig. 5 Reflection and transmission probabilities as functions of magnetic flux ϕ for fixed wavevectors $k = \pi/2$, $\pi/3$, $\pi/4$, $\pi/5$, and $\pi/6$. When the reflection probability $|r_1|$ approaches zero, the system exhibits perfect nonreciprocal transmission, characterized by unit transmission probability on one side and zero transmission on the opposite side.

energy is absorbed by the scattering center, thereby diminishing the efficiency of unidirectional transport. Moreover, we observe that within a finite neighborhood of the blue contour in Fig. 6(a), the transmission remains strongly asymmetric and nearly reflectionless. This behavior implies a degree of robustness to parameter fluctuations. For instance, as shown in Fig. 7, at $\phi_c = \frac{4\pi}{9}$, and $k_c = \frac{\pi}{3}$, the system exhibits $|r_{L_2}| = |r_{R_2}| = 0$, $|t_{R_2}| = 0$, and $|t_{L_2}| < 1$, confirming the presence of an imperfect but clearly directional scattering process.

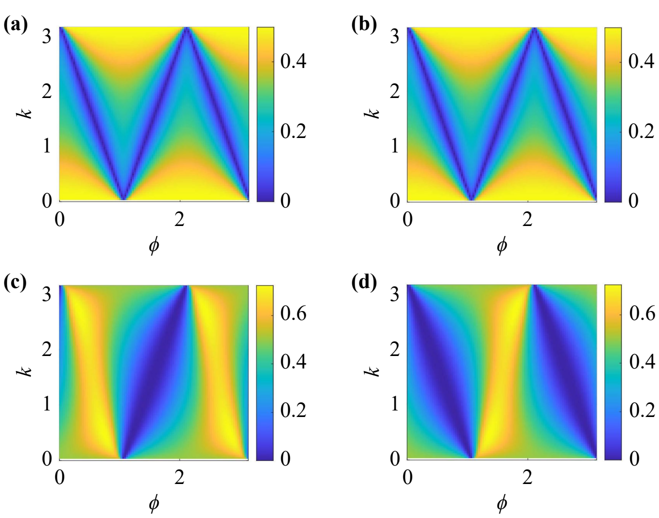

Fig. 6 Scattering probabilities for the asymmetric model under the parameter setting $V_1 = V_2 = V_3 = -e^{i\gamma}$, with $k = \gamma \in (0, \pi)$ and $\phi \in (0, \pi)$. **(a)** Left reflection probability $|r_{L_2}|$; **(b)** Right reflection probability $|r_{R_2}|$; **(c)** Left transmission probability $|t_{L_2}|$; **(d)** Right transmission probability $|t_{R_2}|$. Compared to the previous model, the zero-reflection region (highlighted by the blue curves in the reflection maps) becomes broader. When (k, ϕ) lie near these regions, the system approximately exhibits unidirectional behavior. In these cases, one transmission probability vanishes exactly (e.g., $|t_{L_2}| = 0$ or $|t_{R_2}| = 0$), while the opposite-side transmission is less than unity (e.g., $|t_{R_2}| < 1$ or $|t_{L_2}| < 1$).

iii) Model with central gain and edge loss: $V_1 = V_3 = -V_2 = -e^{i\gamma}$

In this case, the Hamiltonian of the scattering center is given as

$$H_{C_3} = H_{C_1} + e^{i\gamma} b_2^\dagger b_2. \tag{45}$$

The Hamiltonian H_{C_3} satisfies the $\mathcal{PM}_{\mathcal{F}}$ symmetry condition as given in Eq. (14). The corresponding scattering amplitudes are calculated as

$$r_{L_3} = r_{R_3} = -\frac{e^{-2ik}(\cos k + \cos 3\phi)}{2\cos k + 2\cos 3\phi + ie^{-2ik}\sin k}, \tag{46}$$

$$t_{L_3} = -\frac{e^{-ik}(e^{-4i\phi} + e^{2i\phi}e^{-2ik} + 2e^{-i\phi}e^{-ik})}{2(2\cos k + 2\cos 3\phi + ie^{-2ik}\sin k)}, \tag{47}$$

$$t_{R_3} = -\frac{e^{-ik}(e^{4i\phi} + e^{-2i\phi}e^{-2ik} + 2e^{i\phi}e^{-ik})}{2(2\cos k + 2\cos 3\phi + ie^{-2ik}\sin k)}. \tag{48}$$

These expressions satisfy the $\mathcal{PM}_{\mathcal{F}}$-symmetric constraint $t_{L_3}(\phi) = t_{R_3}(-\phi)$ in accordance with Eq. (16). Numerical results are presented in Fig. 8, where the blue contour again marks the condition $|r_{L_3}| = |r_{R_3}| = 0$. From the figure, we observe a striking unidirectional transport regime in which an incoming wave packet from one side experiences no reflection and no transmission, while from the opposite side, the wave is fully transmitted

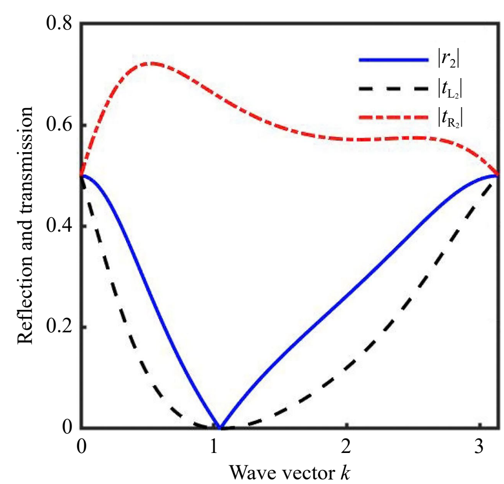

Fig. 7 Scattering probabilities as functions of the wavevector k for the parameter setting $V_1 = V_2 = V_3 = -e^{i\gamma}$, $k = \gamma \in (0, \pi)$, and $\phi_c = 4\pi/9$. Shown are the total reflection probability $|r_2|$ and transmission probabilities $|t_{L_2}|$ and $|t_{R_2}|$. At the critical point $k_c = \pi/3$, the system exhibits unidirectional transparency with $|r_{L_2}| = |r_{R_2}| = 0$, $|t_{L_2}| = 0$, and $|t_{R_2}| \approx 0.65$.

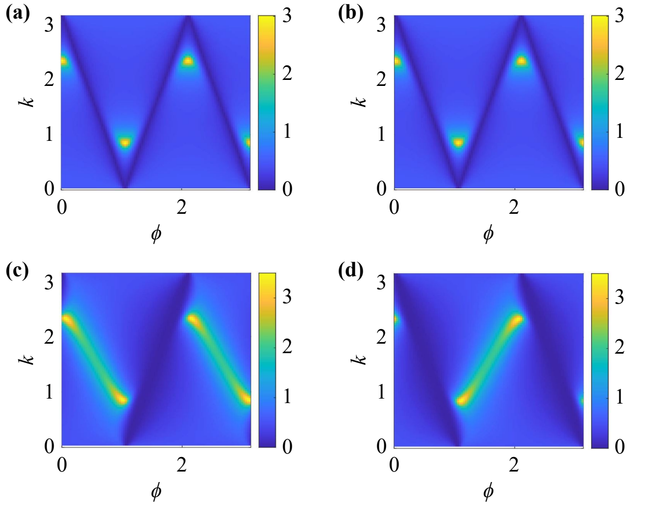

Fig. 8 Scattering probabilities for the asymmetric model with parameters $V_1 = V_3 = -V_2 = -\mathrm{e}^{\mathrm{i}\gamma}$, $k = \gamma \in (0, \pi)$, and $\phi \in (0, \pi)$. Panels show **(a)** the left reflection probability $|r_{\mathrm{L}_3}|$, **(b)** the right reflection probability $|r_{\mathrm{R}_3}|$, **(c)** the left transmission probability $|t_{\mathrm{L}_3}|$, and **(d)** the right transmission probability $|t_{\mathrm{R}_3}|$. When the reflection probabilities approach the blue contour, the system exhibits near-unidirectional transmission with amplification, characterized by $|t_{\mathrm{L}_3}| = 0$ and $|t_{\mathrm{R}_3}| > 1$.

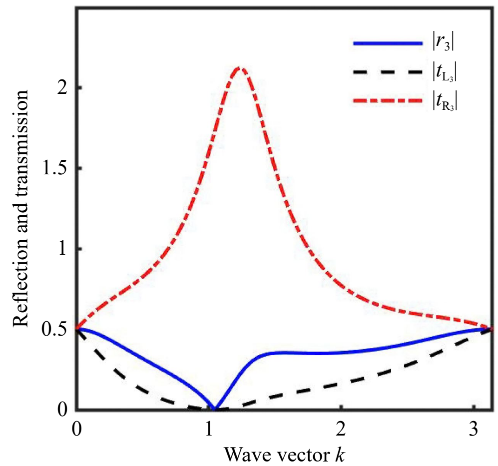

Fig. 9 Scattering probabilities as functions of the wavevector k for the parameter configuration $V_1 = V_3 = -V_2 = -\mathrm{e}^{\mathrm{i}\gamma}$, with $k = \gamma \in (0, \pi)$ and $\phi_{\mathrm{c}} = 4\pi/9$. The plot shows the total reflection probability $|r_3|$ and the left and right transmission probabilities $|t_{\mathrm{L}_3}|$ and $|t_{\mathrm{R}_3}|$. At the critical point $k_c = \pi/3$, the system exhibits a highly nonreciprocal transmission characterized by $|r_{\mathrm{L}_3}| = |r_{\mathrm{R}_3}| = |t_{\mathrm{L}_3}| = 0$ and $|t_{\mathrm{R}_3}| \approx 1.73$, indicating unidirectional amplification.

without reflection. Specifically, for $\phi \in [0, \frac{\pi}{3}] \cup [\frac{2\pi}{3}, \pi]$ and k along the blue curve, this unidirectional behavior is clearly manifested.

Notably, in this model, when $|r_{\mathrm{L}_3}| = |r_{\mathrm{R}_3}| = 0$ and $|t_{\mathrm{R}_3}| = 0$, the transmission amplitude satisfies $|t_{\mathrm{L}_3}| > 1$, and the system exhibits amplification, a hallmark of non-Hermitian scattering in active media. In contrast to Hermitian scattering, where the S-matrix is unitary and total scattering probability is conserved, non-Hermitian systems with gain break unitarity, allowing the sum $|t|^2 + |r|^2$ to exceed unity. This excess corresponds to the net energy injected into the scattering channels by the active elements within the scattering center. From an energy-flow perspective, the amplification is sustained by the gain components, which supply energy to the propagating modes. In our model H_{C_3}, the interplay between spatially distributed gain/loss and magnetic flux creates interference conditions that enable both perfect transmission and net energy amplification. Such behavior aligns with the general framework of non-Hermitian scattering theory, where reciprocity and conservation are no longer guaranteed, and amplification can be engineered via the symmetry-controlled balance of coherent transport and active energy input. Such a configuration can serve as a quantum diode with gain, enabling signal propagation in a single direction while simultaneously amplifying it without backscattering. As shown in Fig. 9, this perfect diode behavior is most pronounced at $\phi_{\mathrm{c}} = \frac{4\pi}{9}$, and $\gamma_{\mathrm{c}} = k_{\mathrm{c}} = \frac{\pi}{3}$.

The non-reciprocity in the above three models all arises from the combined effect of the breaking of time-reversal symmetry (by magnetic flux) and the directional imbalance in dissipation/amplification, both of which are compatible with $\mathcal{PM_F}$ symmetry. The phase γ directly modulates the interference of scattering paths and controls the degree of asymmetry between $|t_L|$ and $|t_R|$. Depending on the specific distribution of non-Hermitian potentials, the strength of nonreciprocity can be either enhanced or suppressed.

4.2.2 Asymmetric complex potentials

iv) Model with asymmetric loss: $V_1 = -V_3 = -\mathrm{e}^{\mathrm{i}\gamma}$, $V_2 = 0$

The scattering center Hamiltonian in this configuration is given by

$$\begin{aligned} H_{\mathrm{C}_4} = & -\mathrm{e}^{-\mathrm{i}\phi}(b_1^\dagger a_{-1} + b_2^\dagger b_1 + a_{-1}^\dagger b_2 \\ & + b_3^\dagger b_2 + a_1^\dagger b_3 + b_2^\dagger a_1) + \mathrm{H.c.} \\ & -\mathrm{e}^{\mathrm{i}\gamma}(b_1^\dagger b_1 - b_3^\dagger b_3), \end{aligned} \tag{49}$$

which explicitly breaks both $\mathcal{PT}$ and $\mathcal{PM_F}$ symmetries. As a result, symmetry arguments alone cannot determine whether this scattering center supports nonreciprocal transport. From the schematic structure, it is evident that the left- and right-incident waves experience asymmetric gain and loss distributions. This suggests that the presence of a magnetic flux, combined with the asymmetric complex potential, may lead to a complete breakdown of reciprocal transmission. To verify this hypothesis, we analytically compute the scattering amplitudes as follows. Eq. (28) is transformed into

$$\begin{aligned}&\alpha_1 = \mathrm{e}^{2\mathrm{i}\phi} + \mathrm{e}^{-\mathrm{i}\phi}\mathrm{e}^{-\mathrm{i}k}, \beta_1 = \mathrm{e}^{-2\mathrm{i}\phi} - \mathrm{e}^{\mathrm{i}\phi}(E+V),\\ &\lambda_1 = 0, \lambda_1' = -\mathrm{e}^{-\mathrm{i}k}(\mathrm{e}^{\mathrm{i}k} - \mathrm{e}^{-\mathrm{i}k}), \varsigma_1 = E\mathrm{e}^{-2\mathrm{i}k},\\ &\mu_1 = 2\mathrm{e}^{2\mathrm{i}k}, \mu_1' = -E\mathrm{e}^{-\mathrm{i}k}, V = -\mathrm{e}^{\mathrm{i}k}. \end{aligned} \tag{50}$$

Under flux reversal $\phi \to -\phi:\ \alpha_1 \to \alpha_1', \beta_1 \to \beta_1'$. Here we define

$$\Omega = \mathrm{e}^{2\mathrm{i}k}[-\alpha_1\alpha_1' E(E+V) - \lambda_1'(\beta_1\beta_1' - E^2\mathrm{e}^{-2\mathrm{i}k})]. \tag{51}$$

The resulting reflection and transmission coefficients are

$$r_{\mathrm{L}_4} = \frac{\alpha_1\alpha_1' E(E+V)}{\Omega}, \tag{52}$$

$$r_{\mathrm{R}_4} = \frac{\lambda_1'(2E\mathrm{e}^{\mathrm{i}k} + \beta_1\beta_1') - 2\alpha_1\alpha_1'\mathrm{e}^{3\mathrm{i}k}(E+V)}{\Omega}, \tag{53}$$

$$t_{\mathrm{L}_4} = \frac{2\mathrm{i}\alpha_1'\beta_1(E+V)\sin k}{\Omega}, \tag{54}$$

$$t_{\mathrm{R}_4} = \frac{2\mathrm{i}\alpha_1\beta_1^{\dagger}(E+V)\sin k}{\Omega}. \tag{55}$$

Despite the absence of symmetry constraints, this model exhibits pronounced nonreciprocal behavior, with the degree of asymmetry strongly dependent on both the flux ϕ and the complex potential parameter γ. At the specific parameter values $\phi_{\mathrm{c}} = \frac{4\pi}{9}$ and $k_{\mathrm{c}} = \frac{\pi}{3}$, we find

$$|r_{\mathrm{L}_4}(k_{\mathrm{c}}, \phi_{\mathrm{c}})| = |r_{\mathrm{R}_4}(k_{\mathrm{c}}, \phi_{\mathrm{c}})| = |t_{\mathrm{R}_4}(k_{\mathrm{c}}, \phi_{\mathrm{c}})| = 0, \tag{56}$$

$$|t_{\mathrm{L}_4}(k_{\mathrm{c}}, \phi_{\mathrm{c}})| = 1. \tag{57}$$

This result demonstrates a perfect unidirectional transmission: a wave incident from the left is fully transmitted with no reflection, while a wave incident from the right is completely blocked. This behavior is illustrated in Fig. 10, where the transmission and reflection probabilities are plotted as functions of the system parameters.

v) Model with purely imaginary antisymmetric gain/loss: $V_1 = -V_3 = -\mathrm{i}\gamma$, $V_2 = 0$

Again, the last model dose not possess $\mathcal{PM}_{\mathcal{F}}$ symmetry, the considered scattering center is given as

$$\begin{aligned} H_{\mathrm{C}_5} = &-\mathrm{e}^{-\mathrm{i}\phi}(b_1^{\dagger}a_{-1} + b_2^{\dagger}b_1 + a_{-1}^{\dagger}b_2\\ &+ b_3^{\dagger}b_2 + a_1^{\dagger}b_3 + b_2^{\dagger}a_1) + \mathrm{H.c.}\\ &-\mathrm{i}\gamma(b_1^{\dagger}b_1 - b_3^{\dagger}b_3), \end{aligned} \tag{58}$$

where the hopping part remains identical to previous models. However, this model has $\mathcal{PT}$ symmetry and is subject to the constraint of Eq. (11). To this end, we give the sacattering solution as

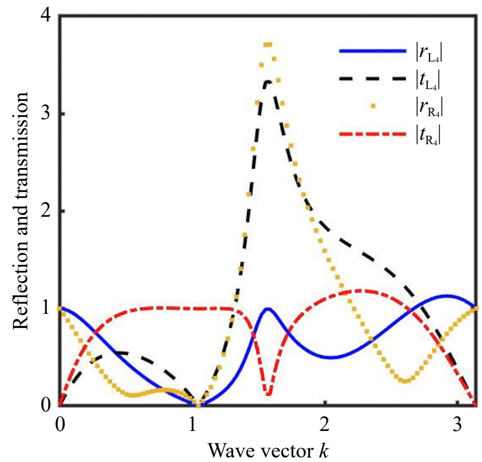

Fig. 10 Scattering probabilities as functions of the wavevector k under the parameter configuration $V_1 = -V_3 = -\mathrm{e}^{\mathrm{i}\gamma}$, $k = \gamma \in (0, \pi)$, and $\phi_{\mathrm{c}} = 4\pi/9$. The plot shows the total reflection probability $|r_{\mathrm{L}_4}|$ and $|r_{\mathrm{R}_4}|$ the transmission probabilities $|t_{\mathrm{L}_4}|$ and $|t_{\mathrm{R}_4}|$. Although the system does not possess $\mathcal{PM}_{\mathcal{F}}$ symmetry, at the critical point $k_{\mathrm{c}} = \gamma_c = \pi/3$, the scattering behavior becomes highly nonreciprocal with $|r_{\mathrm{L}_4}| = |r_{\mathrm{R}_4}| = |t_{\mathrm{R}_4}| = 0$ and $|t_{\mathrm{L}_4}| = 1$, indicating perfect unidirectional transparency.

$$r_{\mathrm{L}_5} = \frac{\lambda_2(\lambda_2^*\varsigma_2 - \rho) - \alpha_2\alpha_2'\lambda_2^*(E - \mathrm{i}\gamma)}{\Omega'}, \tag{59}$$

$$r_{\mathrm{R}_5} = \frac{\lambda_2'(\mu_2\varsigma_2 - \rho) - \alpha_2\alpha_2'\mu_2(E - \mathrm{i}\gamma)}{\Omega'}, \tag{60}$$

$$t_{\mathrm{L}_5} = \frac{-2\mathrm{i}\alpha_2'\alpha_2^*\sin k(E^2 + \gamma^2)}{\Omega'}, \tag{61}$$

$$t_{\mathrm{R}_5} = \frac{-2\mathrm{i}\alpha_2(\alpha_2')^*\sin k(E^2 + \gamma^2)}{\Omega'}, \tag{62}$$

where

$$\begin{aligned} &\alpha_2 = \mathrm{e}^{2\mathrm{i}\phi} - \mathrm{e}^{-\mathrm{i}\phi}(E + \mathrm{i}\gamma), \lambda_2 = \mathrm{e}^{\mathrm{i}k}(\mathrm{e}^{\mathrm{i}k} - \mathrm{i}\gamma),\\ &\mu_2 = \mathrm{e}^{\mathrm{i}k}(\mathrm{e}^{\mathrm{i}k} + \mathrm{i}\gamma), \varsigma_2 = E(2\cos 2k + \gamma^2),\\ &\rho = \alpha_2^*(\alpha_2')^*(E + \mathrm{i}\gamma),\\ &\Omega' = \mathrm{e}^{2\mathrm{i}k}[\alpha_2\alpha_2'\lambda_2^*(E - V_3)\\ &\qquad - \mu_2^*\lambda_2^*\varsigma_2 + \alpha_2^*(\alpha_2')^*\mu_2^*(E + \mathrm{i}\gamma)]. \end{aligned} \tag{63}$$

Under flux reversal $\phi \to -\phi : \alpha_2 \to \alpha_2'$. Clearly,

$$r_{\mathrm{L}_5}(\phi) \neq r_{\mathrm{R}_5}(-\phi), |t_{\mathrm{L}_5}(\phi)| = |t_{\mathrm{R}_5}(\phi)|. \tag{64}$$

This result is consistent with the constraint of $\mathcal{PT}$ symmetry. Numerical simulations are presented in Fig. 11, which reveal distinctive features compared to the previously discussed models. Notably, the left and right transmission probabilities are always equal across the entire parameter space. Moreover, when the parameters fall along the blue curve in the left reflection plot

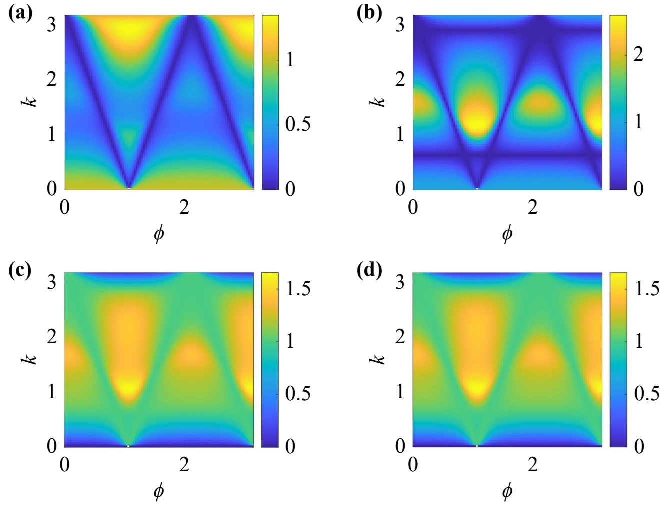

Fig. 11 Scattering probability distributions for the nonreciprocal scattering model with $V_1 = -V_3 = -i\gamma$, $k = \gamma \in (0, \pi)$, and $\phi \in (0, \pi)$. Subfigures show **(a)** the left reflection probability $|r_{L_5}|$; **(b)** the right reflection probability $|r_{R_5}|$; **(c)** the left transmission probability $|t_{L_5}|$; and **(d)** the right transmission probability $|t_{R_5}|$. Although the system lacks $\mathcal{PM_F}$ symmetry, different parameter regimes exhibit distinct transport behaviors. When parameters lie along the blue curve in panel (a), the system behaves reciprocally with $|r_{L_5}| = |r_{R_5}|$ and $|t_{L_5}| = |t_{R_5}|$. In contrast, parameters within the yellow bright region in panel (b) exhibit nonreciprocal reflection $|r_{L_5}| \neq |r_{R_5}|$, while maintaining symmetric transmission $|t_{L_5}| = |t_{R_5}|$.

[Fig. 11(a)], the system exhibits symmetric transport. In contrast, when the parameters lie in the yellow region of the right reflection plot [Fig. 11(b)], pronounced nonreciprocal transmission emerges. This asymmetry originates from the action of the non-Hermitian phase, consistent with the fact that $\mathcal{PT}$ symmetry does not constrain reflection.

The proposal of these two types of models further confirms that nonreciprocal transport is not exclusive to systems with $\mathcal{PM_F}$ symmetry, and $\mathcal{PM_F}$-symmetric systems are only one of the ways to achieve nonreciprocity.

Based on the analysis of five representative configurations, we conclude that systems with general complex potentials can exhibit nonreciprocal transport through the interference between the non-Hermitian phase and the magnetic flux. A robust realization of nonreciprocity, however, requires the cooperative action of spatial symmetry breaking and the non-Hermitian phase. Within this framework, the $\mathcal{PM_F}$ symmetry plays the role of a permissive condition: it enables the possibility of directional transport but does not guarantee its occurrence. By selectively positioning gain and loss at different lattice sites, the system exhibits distinct transport behaviors, including regimes of perfect unidirectional transparency or amplification. These results highlight the critical role of spatial symmetry breaking in engineering nonreciprocal scattering and open new possibilities for controlling light transport in non-Hermitian systems. Our findings provide a theoretical foundation for the design of novel photonic devices such as unidirectional invisible channels and non-Hermitian optical amplifiers.

5 Summary

In this work, we systematically studied the conditions under which nonreciprocal transmission emerges in a class of non-Hermitian lattice systems with finite scattering centers. By introducing complex on-site potentials and magnetic flux into the tight-binding scattering center, we explored how different symmetry classes, especially $\mathcal{PT}$ and $\mathcal{PM_F}$ symmetries, affect the transmission and reflection amplitudes for left and right incident waves.

We first established symmetry-based constraint relations for the scattering matrix and clarified that: while $\mathcal{PM_F}$ symmetry can exhibit nonreciprocity under certain conditions, it is not sufficient to guarantee complete nonreciprocal transport. Nonreciprocity is not ensured by a single symmetry breaking, but arises from the interplay between magnetic flux, non-Hermitian phases, and spatial asymmetry. Notably, systems with $\mathcal{PM_F}$ symmetry demonstrate that symmetric configurations can still support asymmetric transport, which extends the traditional understanding established in $\mathcal{PT}$-symmetric systems.

To validate this, we constructed and analyzed five representative models with different spatial distributions of the complex potentials. By tuning system parameters such as the phase of the magnetic flux and the magnitude of the complex potential, we identified parameter regimes where perfect unidirectional transmission occurs, including reflectionless transmission from one side and complete suppression from the other. In some configurations, we also observed non-Hermitian amplification, which enables gain-assisted diode-like behavior.

It is worth noting that the breaking of the $\mathcal{PM_F}$ symmetry can naturally be linked to the emergence of exceptional points (EPs). In the unbroken phase, the S-matrix eigenvalues remain symmetric with respect to ϕ, and the corresponding eigenstates preserve the $\mathcal{PM_F}$ structure, leading to balanced nonreciprocity. Once the symmetry is spontaneously broken, however, eigenstates lose this constraint and acquire chirality, which strongly enhances directional transport. This suggests that EPs associated with $\mathcal{PM_F}$ symmetry breaking may serve as a robust mechanism to control and amplify nonreciprocal effects. While a detailed study of this phenomenon lies beyond the scope of the present work, we expect that similar physics may be realized in more complex non-Hermitian platforms, providing a promising direction for future investigations.

Appendix A: Full derivation of scattering amplitudes

For completeness, we detail here the derivation of the left- and right-incident scattering amplitudes. Throughout this appendix we keep the notation and parameter definitions used in the main text. The coupled equations for the amplitudes read

$$Ef_{-1} = -\kappa_0 f_{-2} - \mathrm{e}^{\mathrm{i}\phi}\kappa_2 g_1 - \mathrm{e}^{-\mathrm{i}\phi}\kappa_1 g_2, \tag{A1}$$

$$Ef_{1} = -\kappa_0 f_{2} - \mathrm{e}^{-\mathrm{i}\phi}\kappa_2 g_3 - \mathrm{e}^{\mathrm{i}\phi}\kappa_1 g_2, \tag{A2}$$

$$(E-V_1)g_1 = -\mathrm{e}^{\mathrm{i}\phi}\kappa_3 g_2 - \mathrm{e}^{-\mathrm{i}\phi}\kappa_2 f_{-1}, \tag{A3}$$

$$(E-V_3)g_3 = -\mathrm{e}^{\mathrm{i}\phi}\kappa_2 f_1 - \mathrm{e}^{-\mathrm{i}\phi}\kappa_3 g_2, \tag{A4}$$

$$\begin{aligned}(E-V_2)g_2 = & -\mathrm{e}^{-\mathrm{i}\phi}\kappa_3 g_1 - \mathrm{e}^{\mathrm{i}\phi}\kappa_3 g_3 \\ & - \mathrm{e}^{\mathrm{i}\phi}\kappa_1 f_{-1} - \mathrm{e}^{-\mathrm{i}\phi}\kappa_1 f_1.\end{aligned} \tag{A5}$$

Here the lead dispersion is $E = -\kappa_0(\mathrm{e}^{\mathrm{i}k} + \mathrm{e}^{-\mathrm{i}k})$.

Solving Eqs. (A3) and (A4) for g_1 and g_3 gives

$$g_1 = \frac{-\mathrm{e}^{\mathrm{i}\phi}\kappa_3 g_2 - \mathrm{e}^{-\mathrm{i}\phi}\kappa_2 f_{-1}}{(E-V_1)}, \tag{A6}$$

$$g_3 = \frac{-\mathrm{e}^{\mathrm{i}\phi}\kappa_2 f_1 - \mathrm{e}^{-\mathrm{i}\phi}\kappa_3 g_2}{(E-V_3)}. \tag{A7}$$

Substituting these into Eqs. (A1), (A2) and (A5), and rearranging, yields three relations for g_2.

$$g_2 = \frac{[E(E-V_1)-\kappa_2^2]\,f_{-1} + \kappa_0(E-V_1)f_{-2}}{\mathrm{e}^{2\mathrm{i}\phi}\kappa_2\kappa_3 - \mathrm{e}^{-\mathrm{i}\phi}\kappa_1(E-V_1)}, \tag{A8}$$

$$g_2 = \frac{[E(E-V_3)-\kappa_2^2]\,f_{1} + \kappa_0(E-V_3)f_{2}}{\mathrm{e}^{-2\mathrm{i}\phi}\kappa_2\kappa_3 - \mathrm{e}^{\mathrm{i}\phi}\kappa_1(E-V_3)}, \tag{A9}$$

$$g_2 = \frac{(E-V_3)[\mathrm{e}^{-2\mathrm{i}\phi}\kappa_2\kappa_3 - \mathrm{e}^{\mathrm{i}\phi}\kappa_1(E-V_1)]f_{-1} + (E-V_1)[\mathrm{e}^{2\mathrm{i}\phi}\kappa_2\kappa_3 - \mathrm{e}^{-\mathrm{i}\phi}\kappa_1(E-V_3)]f_1}{[(E-V_1)(E-V_2)(E-V_3) - \kappa_3^2(E-V_3) - \kappa_3^2(E-V_1)]}. \tag{A10}$$

Left incidence

For left incidence we use the asymptotic ansatz

$$f_{\mathrm{L}}(j) = \begin{cases}\mathrm{e}^{\mathrm{i}kj} + r_{\mathrm{L}}\mathrm{e}^{-\mathrm{i}kj}, & j \ll -1, \\ t_{\mathrm{L}}\mathrm{e}^{\mathrm{i}kj}, & j \gg 1.\end{cases} \tag{A11}$$

Equating Eqs. (A8) and (A9) and substituting Eq. (A11), one obtains

$$\begin{aligned}&\frac{[E(E-V_1)-\kappa_2^2]f_{-1} + \kappa_0(E-V_1)f_{-2}}{[\mathrm{e}^{2\mathrm{i}\phi}\kappa_2\kappa_3 - \mathrm{e}^{-\mathrm{i}\phi}\kappa_1(E-V_1)]} \\ &\quad = \frac{[E(E-V_3)-\kappa_2^2]f_{1} + \kappa_0(E-V_3)f_{2}}{[\mathrm{e}^{-2\mathrm{i}\phi}\kappa_2\kappa_3 - \mathrm{e}^{\mathrm{i}\phi}\kappa_1(E-V_3)]}.\end{aligned} \tag{A12}$$

For convenience, introduce the shorthand

$$\begin{aligned}\alpha &= \mathrm{e}^{2\mathrm{i}\phi}\kappa_2\kappa_3 - \mathrm{e}^{-\mathrm{i}\phi}\kappa_1(E-V_1), \\ \alpha' &= \mathrm{e}^{-2\mathrm{i}\phi}\kappa_2\kappa_3 - \mathrm{e}^{\mathrm{i}\phi}\kappa_1(E-V_1),\end{aligned} \tag{A13}$$

$$\begin{aligned}\beta &= \mathrm{e}^{-2\mathrm{i}\phi}\kappa_2\kappa_3 - \mathrm{e}^{\mathrm{i}\phi}\kappa_1(E-V_3), \\ \beta' &= \mathrm{e}^{2\mathrm{i}\phi}\kappa_2\kappa_3 - \mathrm{e}^{-\mathrm{i}\phi}\kappa_1(E-V_3),\end{aligned} \tag{A14}$$

$$\lambda = -\kappa_0(E-V_1)\mathrm{e}^{\mathrm{i}k} - \kappa_2^2, \lambda' = -\kappa_0(E-V_1)\mathrm{e}^{-\mathrm{i}k} - \kappa_2^2, \tag{A15}$$

$$\mu = -\kappa_0(E-V_3)\mathrm{e}^{\mathrm{i}k} - \kappa_2^2, \mu' = -\kappa_0(E-V_3)\mathrm{e}^{-\mathrm{i}k} - \kappa_2^2. \tag{A16}$$

The previous relation then reads

$$\begin{aligned}&\frac{\lambda\mathrm{e}^{-\mathrm{i}k} + \lambda' r_{\mathrm{L}}\mathrm{e}^{\mathrm{i}k}}{\alpha} = \frac{\mu' t_{\mathrm{L}}\mathrm{e}^{\mathrm{i}k}}{\beta}, \\ &t_{\mathrm{L}} = \frac{\beta\lambda\mathrm{e}^{-\mathrm{i}k} + \beta\lambda' r_{\mathrm{L}}\mathrm{e}^{\mathrm{i}k}}{\alpha\mu'^{\mathrm{i}k}},\end{aligned} \tag{A17}$$

$$r_{\mathrm{L}} = \frac{\alpha\mu'\mathrm{e}^{\mathrm{i}k}t_{\mathrm{L}} - \beta\lambda\mathrm{e}^{-\mathrm{i}k}}{\beta\lambda'\mathrm{e}^{\mathrm{i}k}}. \tag{A18}$$

Next, equate Eqs. (A9) and (A10). Defining

$$\varsigma \equiv (E-V_1)(E-V_2)(E-V_3) - \kappa_3^2(2E-V_1-V_3), \tag{A19}$$

we obtain

$$\begin{aligned}\frac{\mu' t_{\mathrm{L}}\mathrm{e}^{\mathrm{i}k}}{\beta} &= \frac{(E-V_3)\alpha' f_{-1} + (E-V_1)\beta' f_1}{\varsigma} \\ &= \frac{(E-V_3)\alpha'\mathrm{e}^{-\mathrm{i}k} + r_{\mathrm{L}}\mathrm{e}^{\mathrm{i}k} + (E-V_1)\beta' t_{\mathrm{L}}\mathrm{e}^{\mathrm{i}k}}{\varsigma}.\end{aligned}$$

This yields

$$t_{\mathrm{L}} = \frac{\alpha'\beta(E-V_3)(\mathrm{e}^{-\mathrm{i}k} + r_{\mathrm{L}}\mathrm{e}^{\mathrm{i}k})}{[\varsigma\mu' - \beta\beta'(E-V_1)]\mathrm{e}^{\mathrm{i}k}}, \tag{A20}$$

$$r_{\mathrm{L}} = \frac{[\varsigma\mu' - \beta\beta'(E-V_1)]t_{\mathrm{L}}\mathrm{e}^{\mathrm{i}k} - \alpha'\beta(E-V_3)\mathrm{e}^{-\mathrm{i}k}}{\alpha'\beta(E-V_3)r_{\mathrm{L}}\mathrm{e}^{\mathrm{i}k}}. \tag{A21}$$

Equating Eqs. (A17) and (A20) gives

$$\frac{\beta\lambda \mathrm{e}^{-\mathrm{i}k}+\beta\lambda' r_{\mathrm{L}}\mathrm{e}^{\mathrm{i}k}}{\alpha\mu'\mathrm{e}^{\mathrm{i}k}}=\frac{\alpha'\beta(E-V_3)(\mathrm{e}^{-\mathrm{i}k}+r_{\mathrm{L}}\mathrm{e}^{\mathrm{i}k})}{[\varsigma\mu'-\beta\beta'(E-V_1)]\mathrm{e}^{\mathrm{i}k}},$$
$$r_{\mathrm{L}}=\frac{\lambda[\varsigma\mu'-\beta\beta'(E-V_1)]-\alpha\alpha'\mu'(E-V_3)}{\mathrm{e}^{2\mathrm{i}k}[\alpha\alpha'\mu'(E-V_3)-\lambda'\mu'\varsigma+\beta\beta'\lambda'(E-V_1)]}. \tag{A22}$$

Substituting Eq. (A22) back into Eq. (A17) yields the transmission amplitude

$$t_{\mathrm{L}}=\frac{\beta\lambda \mathrm{e}^{-\mathrm{i}k}+\beta\lambda'\mathrm{e}^{\mathrm{i}k}r_{\mathrm{L}}}{\alpha\mu'\mathrm{e}^{\mathrm{i}k}}$$
$$=\frac{-2\mathrm{i}\kappa_0\alpha'\beta(E-V_1)(E-V_3)\sin k}{\mathrm{e}^{2\mathrm{i}k}[\alpha\alpha'\mu'(E-V_3)-\lambda'\mu'\varsigma+\beta\beta'\lambda'(E-V_1)]}. \tag{A23}$$

Collecting, we obtain the left-incident scattering amplitudes

$$r_{\mathrm{L}}=\frac{\lambda[\varsigma\mu'-\beta\beta'(E-V_1)]-\alpha\alpha'\mu'(E-V_3)}{\mathrm{e}^{2\mathrm{i}k}[\alpha\alpha'\mu'(E-V_3)-\lambda'\mu'\varsigma+\beta\beta'\lambda'(E-V_1)]}, \tag{A24}$$

$$t_{\mathrm{L}}=\frac{-2\mathrm{i}\kappa_0\alpha'\beta(E-V_1)(E-V_3)\sin k}{\mathrm{e}^{2\mathrm{i}k}[\alpha\alpha'\mu'(E-V_3)-\lambda'\mu'\varsigma+\beta\beta'\lambda'(E-V_1)]}. \tag{A25}$$

Right incidence

For right incidence we use

$$f_{\mathrm{R}}^{k}(j)=\begin{cases}t_{\mathrm{R}}^{k}\mathrm{e}^{-\mathrm{i}kj}, & j\ll 0,\\ \mathrm{e}^{-\mathrm{i}kj}+r_{\mathrm{R}}^{k}\mathrm{e}^{\mathrm{i}kj}, & j\gg 0.\end{cases} \tag{A26}$$

Proceeding in complete analogy to the left-incident case, we arrive at

$$r_{\mathrm{R}}=\frac{\lambda'[\mu\varsigma-\beta\beta'(E-V_1)]-\alpha\alpha'\mu(E-V_3)}{\mathrm{e}^{2\mathrm{i}k}[\alpha\alpha'\mu'(E-V_3)-\lambda'\mu'\varsigma+\beta\beta'\lambda'(E-V_1)]}, \tag{A27}$$

$$t_{\mathrm{R}}=\frac{-2\mathrm{i}\kappa_0\alpha\beta'\sin k(E-V_1)(E-V_3)}{\mathrm{e}^{2\mathrm{i}k}[\alpha\alpha'\mu'(E-V_3)-\lambda'\mu'\varsigma+\beta\beta'\lambda'(E-V_1)]}. \tag{A28}$$

Parameter mapping under $\phi\to-\phi$ and $k\to-k$

In the shorthand definitions given in Eq. (A16), one can verify the mapping

$$\phi\to-\phi:\ \ \alpha\to\alpha',\beta\to\beta';\ \ k\to-k:\ \ \lambda\to\lambda',\mu\to\mu'. \tag{A29}$$

References

1. N. Nagaosa and Y. Yanase, Nonreciprocal transport and optical phenomena in quantum materials, *Annu. Rev. Condens. Matter Phys.* 15(1), 63 (2024)
2. Y. Avni, M. Fruchart, D. Martin, D. Seara, and V. Vitelli, Nonreciprocal Ising model, *Phys. Rev. Lett.* 134(11), 117103 (2025)
3. H. Ghaemi-Dizicheh, and H. Schomerus, Compatibility of transport effects in non-Hermitian nonreciprocal systems, *Phys. Rev. A* 104(2), 023515 (2021)
4. H. Ghaemi-Dizicheh, Transport effects in non-Hermitian nonreciprocal systems: General approach, *Phys. Rev. B* 107(12), 125155 (2023)
5. L. Wang, Z. Yi, L. H. Sun, and W. J. Gu, Nonreciprocal two-photon transmission and statistics in a chiral waveguide QED system, *Chin. Phys. B* 31(5), 054206 (2022)
6. X. Q. Li, X. Z. Zhang, G. Zhang, and Z. Song, Asymmetric transmission through a flux controlled non-Hermitian scattering center, *Phys. Rev. A* 91(3), 032101 (2015)
7. C. Li, L. Jin, and Z. Song, Non-Hermitian interferometer: Unidirectional amplification without distortion, *Phys. Rev. A* 95(2), 022125 (2017)
8. X. Z. Zhang, L. Jin, and Z. Song, Perfect state transfer in PT-symmetric non-Hermitian networks, *Phys. Rev. A* 85(1), 012106 (2012)
9. J. Li, Y. Yang, X. W. Xu, J. Lu, H. Jing, and L. Zhou, Nonreciprocal single-photon band structure in a coupled-spinning-resonator chain, *Opt. Express* 33(2), 2487 (2025)
10. X. Zhang, H. Li, R. Zeng, M. Hu, M. Xu, X. Zhou, Y. Lan, X. Xia, J. Xu, and Y. Yang, Nonreciprocal single-photon scattering mediated by a driven Λ-type three-level giant atom, *Commum. Theor. Phys.* 76(11), 115501 (2024)
11. X. Huang, C. Lu, C. Liang, H. Tao, and Y. C. Liu, Loss-induced nonreciprocity, *Light Sci. Appl.* 10(1), 30 (2021)
12. M. A. Huang, W. B. Hu, and F. M. Bai, Surface acoustic wave-spin wave coupling and magneto-acoustic nonreciprocal devices, *Acta Phys. Sin.* 73(15), 158501 (2024)
13. X. Cao, A. Irfan, M. Mollenhauer, K. Singirikonda, and W. Pfaff, Parametrically controlled chiral interface for superconducting quantum devices, *Phys. Rev. Appl.* 22(6), 064023 (2024)
14. D. W. Liu, Z. H. Li, S. L. Chao, Y. Wu, and L. G. Si, Dynamical switchable quantum nonreciprocity induced by off-resonant chiral two-photon driving, *Sci. China Phys. Mech. Astron.* 67(6), 260313 (2024)
15. L. Mercier de Lépinay, C. F. Ockeloen-Korppi, D. Malz, and M. A. Sillanpää, Nonreciprocal transport based on cavity Floquet modes in optomechanics, *Phys. Rev. Lett.* 125(2), 023603 (2020)
16. M. Wang, R. Y. Zhang, C. Zhang, H. Xue, H. Jia, J. Hu, D. Wang, T. Jiang, and C. T. Chan, Three-dimensional

nonreciprocal transport in photonic topological heterostructure of arbitrary shape, *Sci. Adv.* 11(2), eadq9285 (2025)

17. S. T. Huang, Y. B. Qian, Z. Y. Zhang, L. Sun, B. P. Hou, and L. Tang, Nonreciprocal photon transport in a chiral optomechanical system, *Adv. Quantum Technol.* 7(11), 2400217 (2024)
18. X. J. Sun, W. X. Liu, H. Chen, and H. R. Li, Tunable single-photon nonreciprocal scattering and targeted router in a giant atom-waveguide system with chiral couplings, *Commum. Theor. Phys.* 75(3), 035103 (2023)
19. X. W. Xu, Y. Li, B. Li, H. Jing, and A. X. Chen, Nonreciprocity via nonlinearity and synthetic magnetism, *Phys. Rev. Appl.* 13(4), 044070 (2020)
20. S. A. Biehs and G. S. Agarwal, Enhancement of synthetic magnetic field induced nonreciprocity via bound states in the continuum in dissipatively coupled systems, *Phys. Rev. B* 108(3), 035423 (2023)
21. H. Li, X. Zhang, R. Zeng, M. Hu, M. Xu, X. Zhou, X. Xia, J. Xu, and Y. Yang, Dynamic tunable nonreciprocal single-photon scattering mediated by a giant atom assisted with a time-modulated cavity, *Opt. Express* 32(22), 38292 (2024)
22. Y. Liu, X. T. Xu, M. He, H. T. Zhao, et al, Nonreciprocal transport in the superconducting state of the chiral crystal $NbGe_2$, *Chin. Phys. B* 33(5), 057402 (2024)
23. X. J. Sun, W. X. Liu, H. Chen, C. Y. Wang, H. Z. Ma, and H. R. Li, Single-photon transport in a waveguide-cavity-emitter system, *Int. J. Theor. Phys.* 61(8), 216 (2022)
24. Y. Hu, W. Z. Jia, and C. H. Yan, Single-photon switches, beam splitters, and circulators based on the photonic Aharonov-Bohm effect, *Opt. Express* 31(7), 11142 (2023)
25. X. F. Chen, P. J. Hu, A. M. Guo, T. F. Fang, and C. Jia, Controllable nonreciprocal spin Seebeck effect in helimagnets, *New J. Phys.* 27(5), 053504 (2025)
26. W. Chen, D. Leykam, Y. D. Chong, and L. Yang, Nonreciprocity in synthetic photonic materials with nonlinearity, *MRS Bull.* 43(6), 443 (2018)
27. T. Kokkeler, I. Tokatly, and F. S. Bergeret, Nonreciprocal superconducting transport and the spin Hall effect in gyrotropic structures, *SciPost Phys.* 16(2), 055 (2024)
28. L. Wang, Y. Z. Jing, K. W. Xiao, and W. Y. Wang, Nonreciprocal quantum transport of ultracold atoms in a driven quadruple-well potential with synthetic gauge fields, *Phys. Scr.* 100(5), 055113 (2025)
29. Y. Z. Jing, K. W. Xiao, Y. Q. Ma, F. Q. Dou, and W. Y. Wang, Nonreciprocal dynamics of exceptional points in pseudo-Hermitian systems under artificial gauge field, *New J. Phys.* 27(3), 033015 (2025)
30. Y. Chen, Y. L. Zhang, Z. Shen, C. L. Zou, G. C. Guo, and C. H. Dong, Synthetic gauge fields in a single optomechanical resonator, *Phys. Rev. Lett.* 126(12), 123603 (2021)
31. M. Lei, P. Jin, Y. Zhou, Y. Li, L. Xu, and J. Huang, Reconfigurable, zero-energy, and wide-temperature loss-assisted thermal non-reciprocal metamaterials, *Proc. Natl. Acad. Sci. USA* 121(44), e2410041121 (2024)
32. Y. X. Wang, C. Wang, and A. A. Clerk, Quantum nonreciprocal interactions via dissipative gauge symmetry, *PRX Quantum* 4(1), 010306 (2023)
33. J. Ma, H. Wang, W. Zhuo, B. Lei, S. Wang, W. Wang, X. Y. Chen, Z. Y. Wang, B. Ge, Z. Wang, J. Tao, K. Jiang, Z. Xiang, and X. H. Chen, Field-free Josephson diode effect in $NbSe_2$ van der Waals junction, *Commun. Phys.* 8(1), 125 (2025)
34. Y. Maleki, C. F. Zhou, and M. S. Zubairy, Time-reversal-symmetry breaking in a scalable cavity QED lattice, *Phys. Rev. A* 108(6), 063709 (2023)
35. Y. Q. Li, H. Y. Du, Y. F. Wang, J. Liang, L. Xiao, W. Yi, J. Ma, and S. Jia, Observation of frustrated chiral dynamics in an interacting triangular flux ladder, *Nat. Commun.* 14(1), 7560 (2023)
36. O. Gargiulo, S. Oleschko, J. Prat-Camps, M. Zanner, and G. Kirchmair, Fast flux control of 3D transmon qubits using a magnetic hose, *Phys. Lett.* 118(1), 012601 (2021)
37. I. T. Rosen, S. Muschinske, C. N. Barrett, A. Chatterjee, M. Hays, M. A. DeMarco, A. H. Karamlou, D. A. Rower, R. Das, D. K. Kim, B. M. Niedzielski, M. Schuldt, K. Serniak, M. E. Schwartz, J. L. Yoder, J. A. Grover, and W. D. Oliver, A synthetic magnetic vector potential in a 2D superconducting qubit array, *Nat. Phys.* 20(12), 1881 (2024)